SANDIA REPORT
SAND2018-14089
Unlimited Release
Printed December 2018

Modeling Radionuclide Releases from TRISO Particles by Simultaneous Diffusion Through, and Corrosion of, the Silicon Carbide Barrier Layer

Fred Gelbard and David Sassani

Prepared by
Sandia National Laboratories
Albuquerque, New Mexico 87185 and Livermore, California 94550

Sandia National Laboratories is a multimission laboratory managed and operated by National Technology and Engineering Solutions of Sandia, LLC, a wholly owned subsidiary of Honeywell International, Inc., for the U.S. Department of Energy's National Nuclear Security Administration under contract DE-NA0003525.

Issued by Sandia National Laboratories, operated for the United States Department of Energy by National Technology and Engineering Solutions of Sandia, LLC.

NOTICE: This report was prepared as an account of work sponsored by an agency of the United States Government. Neither the United States Government, nor any agency thereof, nor any of their employees, nor any of their contractors, subcontractors, or their employees, make any warranty, express or implied, or assume any legal liability or responsibility for the accuracy, completeness, or usefulness of any information, apparatus, product, or process disclosed, or represent that its use would not infringe privately owned rights. Reference herein to any specific commercial product, process, or service by trade name, trademark, manufacturer, or otherwise, does not necessarily constitute or imply its endorsement, recommendation, or favoring by the United States Government, any agency thereof, or any of their contractors or subcontractors. The views and opinions expressed herein do not necessarily state or reflect those of the United States Government, any agency thereof, or any of their contractors.

Printed in the United States of America. This report has been reproduced directly from the best available copy.

Available to DOE and DOE contractors from
U.S. Department of Energy
Office of Scientific and Technical Information
P.O. Box 62
Oak Ridge, TN 37831

Telephone: (865) 576-8401
Facsimile: (865) 576-5728
E-Mail: reports@osti.gov
Online ordering: http://www.osti.gov/scitech

Available to the public from
U.S. Department of Commerce
National Technical Information Service
5301 Shawnee Rd
Alexandria, VA 22312

Telephone: (800) 553-6847
Facsimile: (703) 605-6900
E-Mail: orders@ntis.gov
Online order: https://classic.ntis.gov/help/order-methods/

SAND2018-14089
Printed December 2018
Unlimited Release

Modeling Radionuclide Releases from TRISO Particles by Simultaneous Diffusion Through, and Corrosion of, the Silicon Carbide Barrier Layer

Fred Gelbard and David Sassani
Nuclear Safety Assessment and
Nuclear Waste Disposal Research and Analysis
Sandia National Laboratories
P. O. Box 5800
Albuquerque, New Mexico 87185-MS0490

Abstract

TRISO nuclear fuel particles that are less than 1 mm in diameter are designed with multiple barrier layers to retain fission products both during reactor operations and for long-term geological disposal. The primary barrier is a 35 μm thick silicon carbide (SiC-a highly impermeable semi-metal) layer for which data are available on the diffusion of short-lived fission products at high temperatures (> 1000 °C). However, for a geological repository, this layer may contact brine and hence corrode even at ambient temperatures. As an initial approach to assess the effectiveness of the SiC barrier for geological repositories, ranges of fission product diffusivities and corrosion rates for SiC are modeled concurrently with the simultaneous effect of radioactive decay. Using measured corrosion rates of SiC, if the diffusivity is more than about 10^{-20} m^2/s, fission product releases may occur before the SiC barrier has corroded to the point of breach. For diffusivities less than about 10^{-21} m^2/s there may not be significant diffusional releases prior to SiC barrier removal/breach by corrosion. This work shows the importance of estimating diffusivities in SiC at geological repository temperatures, and highlights the relevance of evaluating the porosity/permeability evolution of the SiC layer in a geologic environment.

ACKNOWLEDGMENTS

This work was supported by the U.S. Department of Energy Office of Nuclear Energy, through the Office of Spent Fuel and Waste Science and Technology (SFWST) Research and Development (DOE NE-81) within the Spent Fuel and Waste Disposition Campaign. The authors acknowledge our gratitude to Philippe Weck (SNL), Ed Matteo (SNL), Peter Swift (SNL), Kevin McMahon (SNL), and Robert MacKinnon (SNL) for discussions on technical aspects and integration of this work. In addition, the authors thank Mark Tynan (DOE NE-81), Joe Price (DOE NE-81), Bill Spezialetti (DOE NE-81), Tim Gunter (DOE NE-81) and William Boyle (DOE NE-8) for their discussions, oversight and guidance on topics covered in this report. A draft of this report was improved by the technical reviews of Emily Stein (SNL), Allen Ricks (SNL), and Peter Swift (SNL).

Table of Contents

Table of Figures

Table of Tables

NOMENCLATURE

Abbreviation	Definition
A	outer surface area of corroding barrier (m^2)
C	fission product concentration in barrier (kg/m^3)
C_1	fission product concentration in core (kg/m^3)
$C_1(0)$	initial fission product concentration in core (kg/m^3)
$\mathcal{D}$	fission product diffusivity in SiC barrier (m^2/s)
$\mathcal{D}_{core}$	fission product diffusivity in core consisting of the UO_2 kernel, and the layers of porous pyrolytic carbon and inner pyrolytic carbon (m^2/s)
F	retained mass fraction of radionuclide in core and barrier system
FP	fission product
h	spacing in ξ coordinate
H	barrier layer thickness (m)
IPyC	inner pyrolytic carbon
k	corrosion rate ($kg/m^2/s$)
L	initial barrier layer thickness (m)
M	radionuclide mass in core and barrier (kg)
m	barrier mass (kg)
MOX	mixed oxide fuel
OPyC	outer pyrolytic carbon layer
P	defined as $rC\exp(\lambda t)$ (kg/m^2)
r	radial coordinate (m)
R_1	inner barrier radius (m)
R_2	outer barrier radius (m)
SiC	silicon carbide
t	time (s)
$t_{1/2}$	half-life (years)
T	time (s)
ThO_2	thorium oxide fuel
TRISO	**Tri**structural-**Iso**tropic

Abbreviation	Definition
UO_2	uranium oxide fuel
V	recession velocity due to corrosion (m/s)
Δt	time step (s)
λ	fission product decay rate, equal to ln(2)/half-life (s^{-1})
ξ	normalized dimensionless spatial coordinate
ρ	material density of SiC barrier layer (3180 kg/m^3)
τ_{diff}	diffusion time-scale (s)
τ_{corr}	corrosion time-scale (s)
τ_{dec}	radioactive decay time-scale (s)

This page is intentionally blank.

I. Introduction

TRISO (**Tri**structural-**Iso**tropic) fuel consists of numerous coated fuel particles, slightly less than 1 mm in diameter, that are embedded in cylindrical blocks or spheres of graphite. The particles consist of a spherical kernel of fuel, such as UO_2, that is about 500 μm in diameter, and four coating layers as shown schematically in a cut-away view in Figure 1. The purpose of each layer is given in Nabielek et al. [2010], and summarized below in Table 1. These layers in order away from the UO_2 are: (1) a buffer layer of porous pyrolytic carbon, (2) an inner dense pyrolytic carbon (IPyC) layer, (3) a silicon carbide (SiC) layer, and (4) an outer dense pyrolytic carbon (OPyC) layer.

As shown in Figure 2 and discussed by Van den Akker and Ahn [2013], about 5,580 TRISO particles are embedded in graphite compacts (graphite cylinders 4.928 cm long and 1.245 cm in diameter), as shown in the center image. Figure 2 also shows the hexagonal fuel elements in the rightmost image. The fuel elements are hexagonal graphite blocks with 324 holes, 216 of which are filled with compacts (and some containing alignment dowels), and 108 holes are used for coolant flow. There is a total of 3,126 compacts per fuel element. The fuel elements are 79.3 cm tall and 36 cm wide flat-to-flat. An alternative fuel design has the TRISO particles embedded in graphite spheres called pebbles (analogous to compacts), which are 6 cm in diameter [e.g., Fachinger et al., 2006].

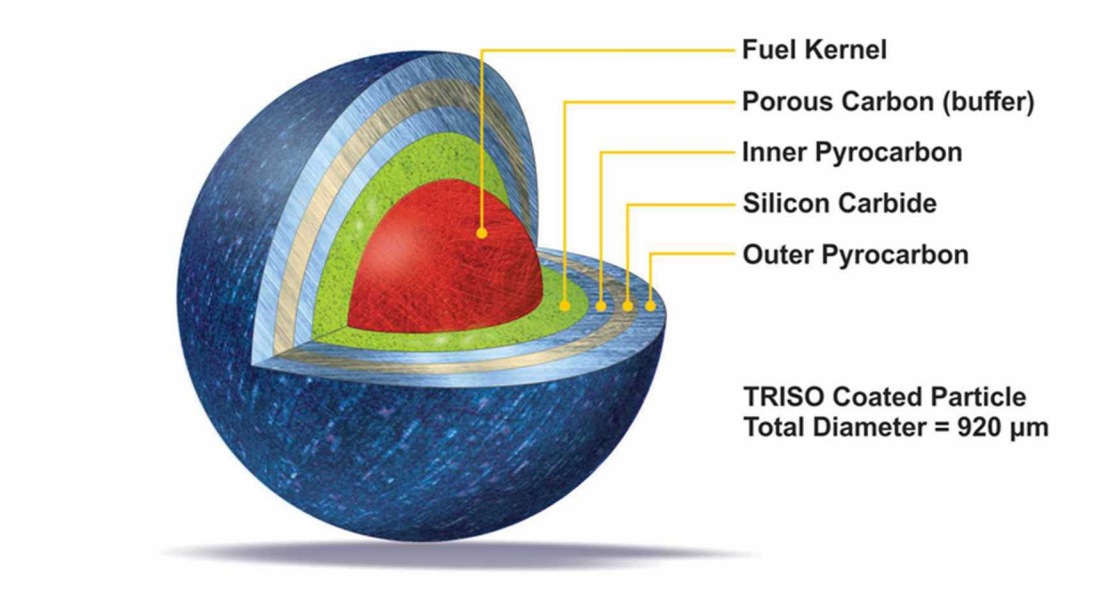

Figure 1. Schematic drawing of a TRISO fuel particle (not to scale) with four protective layers (pyrocarbon = pyrolytic carbon) [from Sassani et al., 2018].

Table 1. Characteristics of TRISO fuel particle with a UO_2 core of radius 250 μm[a]

Layer	Thickness (μm)	Purpose
porous pyrolytic carbon buffer	95	- allows kernel to swell under irradiation - stops recoiling fission products from reaching SiC layer - provides void volume for gases
inner dense pyrolytic carbon (IPyC)	40	- barrier to gaseous fission products - slows down metallic fission product transport
Silicon Carbide (SiC)	35	- main fission product barrier retaining all gaseous and metallic fission products to a very high extent - structural support to contain gas pressure
Outer dense pyrolytic carbon (OPyC)	40	- protects SiC layer from chemical and mechanical damage - adds to support to contain gas pressure

[a]Sources: Fachinger et al. [2006] and Nabielek et al. [2010].

Figure 2. TRISO coated particles (left) are formed into fuel compacts (center) and inserted into graphite fuel elements (right). Taken from Sterbentz et al. [2004].

Two studies [Fachinger et al., 2006; Van den Akker and Ahn, 2013] have evaluated the potential releases from TRISO spent fuel in geologic repository environments. Fachinger et al., [2006] conducted experiments to measure hydrologic properties (i.e., porous media diffusivities) and corrosion rates for the various materials of the TRISO fuel pebbles/particles in a number of fluid compositions at relevant temperatures. The measurements were made on separated materials rather than intact pebbles or particles. The diffusive transport behavior was measured for the graphite matrix (i.e., from the pebble) using isotopes of hydrogen, chlorine, strontium, and cesium. Corrosion rates were measured for the graphite matrix, the SiC (non-irradiated and irradiated), and the pyrocarbon [Fachinger et al., 2006]. Fachinger et al. [2006] also measured leaching rates of ThO_2, UO_2, and (Th-U) mixed oxide (MOX) fuel kernels in various fluids over a range of redox conditions.

The conclusions of Fachinger et al. [2006] included (a) the graphite matrix of the pebble serves as a porous medium that reduces water contact with the TRISO particles, (b) porous media diffusion is the primary transport mechanism through the graphite matrix of the pebble, (c) pyrocarbon and SiC layers have lifetimes from 1000's to 100,000's years depending on conditions (temperature, fluid composition, radiation dose), and (d) fuel kernels may have relatively long lifetimes (≥100,000's years) depending on conditions. Their study also recommended further work evaluating (a) the porous media behavior of the graphite matrix and how it changes due to graphite corrosion, (b) the effect of internal pressure build-up on the layer lifetime, (c) mass transport through the graphite matrix, and (d) development of an integrated model of the total set of processes.

In the second study, Van den Akker and Ahn [2103] constructed a performance assessment of hexagonal graphite fuel elements (with TRISO particles in graphite compacts) degrading within an unsaturated (oxidizing) geologic repository system. The primary waste form barrier in that work was the graphite matrix of the fuel element (or the graphite matrix of the compact in a second scenario), which slowly oxidatively corrodes to release radionuclides uniformly over tens of millions of years. That study evaluated stochastic failure (rupture) of the SiC layer of the TRISO particle due to combined effects of SiC corrosion and internal pressure build-up from helium generation. Their analyses included statistical variability of the SiC strength, and concluded that, if protection by the OPyC layer is ignored, then lifetimes on the order of thousands to hundreds of thousands of years were expected. Although Van den Akker and Ahn [2013] estimated that protection by the OPyC layer could extend SiC layer lifetime to millions of years, they made the simplifying assumption that the particle lifetime was short compared to graphite matrix corrosion (of either the fuel element or the compact). Hence for their model they assumed the TRISO particles had released all radionuclides and distributed those radionuclides uniformly throughout their spherical approximations (of either the entire fuel element or just of a single graphite compact) of corroding graphite. The corrosion of the graphite sphere was then used to assess radionuclide releases from the TRISO fuel directly to the host rock.

As recommended by Fachinger et al. [2006], we have begun the construction of a quantitative integrated model on the scale of a fuel compact. Our integrated model includes major features, events, and processes to evaluate stochastically the release of radionuclides under varying repository conditions through time. In this report we present our analyses of the primary coupled process considerations for the SiC layer of the TRISO particles. The analyses assess the relevance of these processes at repository conditions. Future work will consider uncertainties in material properties for the porous media transport processes. This will include assessment of whether or not the SiC layer porosity would render it effectively impermeable until after corrosion breach, as well as parametric uncertainties in the material properties of the other layers to the extent data are available.

Numerous studies have been reported on measuring radionuclide releases from TRISO fuel under reactor conditions [Friedland et al., 2009; Friedland et al., 2011; Demkowicz et al., 2013; Kirchhofer et al., 2013; Chaou et al., 2014; Deng et al., 2015; Demkowicz et al., 2016; Hunn et al., 2016; Morris et al., 2016; Bower et al., 2017; Cao et al., 2017], and modeling these processes [Miller et al., 2002; Boer et al., 2010; Powers and Wirth, 2010; Khalil et al., 2011]. For these studies the fuel may attain an operating temperature of 1200 °C. However, under geological repository conditions the temperatures are much lower, and the fuel will evolve over much longer time than operations in the reactor.

In a previous study [Gelbard, 2003, and see the update in Appendix A of this work], we showed that an exact analytical solution can be obtained for the transient diffusion of a fission product through a multilayer TRISO particle. For that analysis, the layer thicknesses were constant. We now consider the effects of barrier layer corrosion while the fission product is simultaneously radioactively decaying and diffusing through the barrier layer. Barrier corrosion creates a moving-boundary diffusion problem.

Transport within a domain with a moving boundary is a well-studied problem [Kucera, 1985; Tao, 1986; Crank, 1988; Shyy, 2007]. But we have not found such analysis for TRISO fuel. In this work we apply the analysis techniques developed for heat conduction with an ablating surface to a corroding diffusion barrier. In particular, our problem is simpler because the corrosion rate is independent of the fission product concentration. This results in a linear system of equations for each time step that does not require an iterative solution.

We begin in Section II by discussing the release mechanisms from TRISO fuel particles. Estimates of the time-scales for corrosion, diffusion and radioactive decay are given in terms of simple expressions. Nonetheless, these expressions are later shown to be fairly useful at estimating the relative timing of these three processes on fission product release. In Section III, the model is presented of a core region that has a uniform fission product concentration, enclosed within a barrier of SiC that provides a diffusion barrier for fission products. Because of corrosion, the SiC barrier thickness decreases with time, thus resulting in a moving-boundary problem. The moving-boundary problem is reduced to a fixed-boundary problem using two

transformations that are derived in detail. In Section IV the numerical discretization of the coupled partial differential and ordinary differential equations is given in detail. In Section V the mass fraction of released fission product is given for a broad range of fission product diffusivities in SiC. This broad range is necessary since data have not been found for the radionuclides of interest at the temperature of interest. We conclude in Section VI with observations from this work of a bounding value for the fission product diffusivity. Diffusivities larger than the bounding value indicate that if brine contacts the SiC barrier, diffusion may release fission products before the barrier has corroded. However, for diffusivities that are smaller than the bounding value, then diffusive releases will be minimal until the barrier is removed/breached by corrosion. This conclusion may be different if the properties of SiC allow porous media processes to occur prior to corrosion breach at expected repository temperatures. In our future work, we will evaluate the potential for such processes in SiC and delineate the range of potential radionuclide release via aqueous diffusive pathways in a model that integrates quantitatively porous media behavior of the TRISO particle layers and the surrounding compact matrix graphite.

This page is intentionally blank

II. Evaluation of release mechanisms for non-ruptured TRISO particles – consideration of geologic repository environment

For release analysis, we assume that all the layers remain intact upon removal from the reactor, and the fuel has cooled to a temperature that is far below the maximum fuel operating temperature of 1200 °C. Ruptures/fractures of the SiC layer would permit faster pathways for radionuclide release, which may substantially decrease its barrier function for containment. Continuing radioactive decay will keep the fuel temperature above the ambient temperature, but after at most about 2,000 years (depending on fuel enrichment and burnup, and repository thermal design), the fuel is close to the ambient repository temperature. Even for initially intact layers, there are three mechanisms that are considered here for release of fission products: (1) helium pressure buildup that could rupture the main barrier which is the SiC layer [Van den Akker and Ahn, 2013], (2) generalized bulk diffusive transport through the layer, and (3) aqueous corrosion of the layer. These processes are not totally independent. Corrosion reduces the layer thickness, which may reduce the effective tensile strength to retain pressure within the particle, and thus facilitate layer rupture. Corrosion also results in thinner layers which decreases the diffusive transport path length. In this work we consider the coupled processes of barrier corrosion, diffusion of fission products through a corroding barrier, and radioactive decay. Although the SiC layer is chosen as the barrier, the analysis in this work is general. The analysis may be used for any system of a corroding barrier that acts to retain any radionuclide in the core region, which has a much shorter diffusion time-scale than that in the barrier. As shown by Fachinger et al. [2006], measurements of porous media diffusivities for graphite and pyrolytic carbon are much higher than the threshold values constrained below for effective bulk diffusion through SiC versus SiC corrosion. Future work implementing our integrated conceptual model will evaluate the SiC layer for its potential porous media properties prior to corrosion thinning/breach and explicitly include porous media diffusion through the other layers.

The corrosion rate of irradiated SiC and pyrolytic carbon in different aqueous solutions has been reported by Fachinger et al. [2006]. Their data are plotted in Figure 3 in this work from their Table 5 and Table 3, respectively. The cumulative probability for total failure of the SiC layer due to stress and corrosion according to Van den Akker and Ahn [2013] varies between 7,000 years and 1.4×10^5 years for SiC corrosion rates of 4.09×10^{-5} g/m^2/day and 2.03×10^{-6} g/m^2/day, respectively. Assuming corrosion without stress, these same corrosion rates would lead to SiC layer lifetimes of 7,500 years and 1.5×10^5 years, respectively, by using Eq. (II.5) as given below. Thus corrosion with pressure buildup that may fail the SiC layer, reduces SiC barrier lifetime by less than 10% compared to SiC layer lifetime just due to corrosion without pressure buildup. As shown in Figure 3, the aqueous corrosion rate of pyrolytic carbon at 90 °C is 2.2×10^{-7} g/m^2/day at atmospheric oxygen levels and is more than two orders of magnitude slower than that for SiC at the same temperature. Thus if the OPyC layer remains intact, it may provide substantial protection of the SiC barrier to corrosion by aqueous solutions such that the SiC layer may have a lifetime of up to 2×10^6 years [Van den Akker and Ahn, 2013], which is substantial for performance time frames of a geologic repository. In most geologic systems, the

OPyC layer would likely become saturated with the aqueous phase, but would substantially reduce the contact area on the SiC. Even without corrosion of the SiC, diffusion through the SiC barrier still needs to be considered.

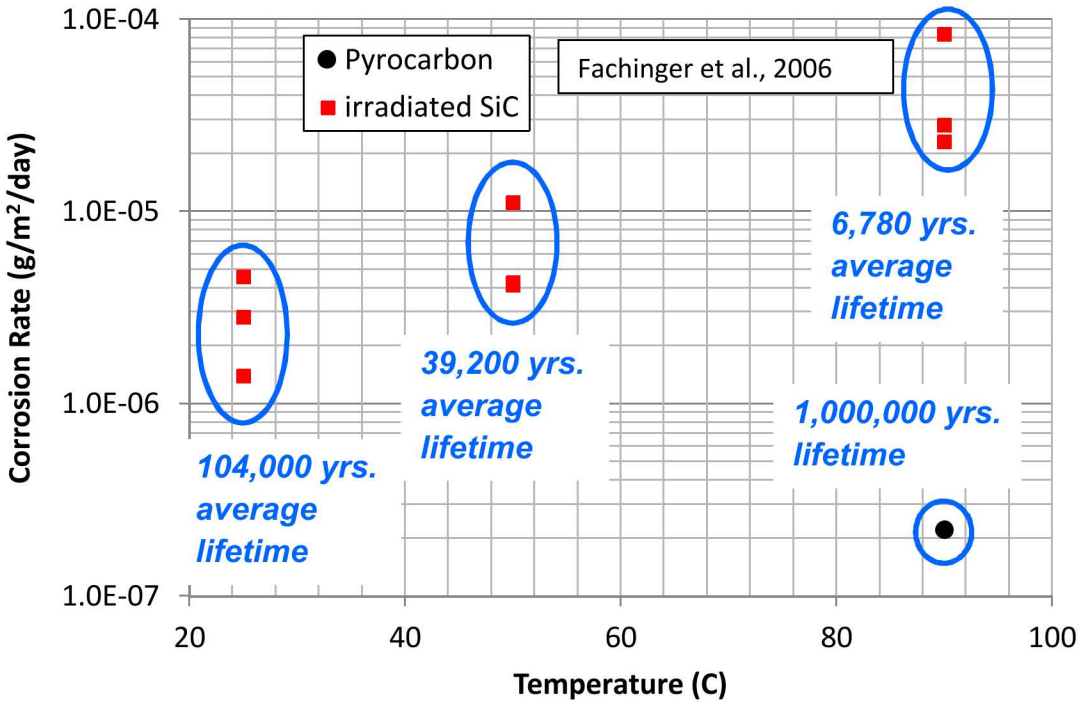

Figure 3. Data from Fachinger et al., [2006] for aqueous corrosion rates of SiC at various temperatures for different brines. For the average aqueous corrosion rate at 25 °C, a 35 micrometer thick SiC layer lasts ~100,000 years, and at 90 °C the layer lasts ~7000 years. Aqueous corrosion rate for OPyC at 90 °C shown for comparison and corresponds to lifetime of ~1,000,000 years.

Diffusion data at high temperatures in SiC have been collected by Malherbe [2013], but we found no diffusion data in SiC for any of the radionuclides given in Table 2 at repository temperatures. Data for diffusion of ^{36}Cl, ^{90}Sr, and ^{134}Cs through graphite in different brines range from 1.2×10^{-13} m^2/s to 6.3×10^{-13} m^2/s [Fachinger et al., 2006]. For non-corroding layers, the problem of determining radionuclide releases by diffusion has been reported by Gelbard [2003]. The challenge is that the diffusivities of radionuclides in Table 2 through SiC and pyrolytic carbon need to be estimated. Such basic principles calculations have been reported for radionuclides by De Bellefon and Wirth [2011], Ko et al. [2016], Minato et al. [1994], Rabone et al. [2014], and Rabone and Lopez-Honorato [2015], and should be considered in future work for the fission products in Table 2 at repository temperatures.

For this work we establish what are the minimum diffusivities in SiC for which diffusional releases are significant. Thus, accurate diffusivities may not be needed if the diffusivities can be shown to be bounded to be below the minimum diffusivity to be important relative to corrosion.

Table 2. Some radionuclides (Rn) of interest for geological repositories.

Rn	**Half-life $t_{1/2}$ (years)**	**$\lambda = \frac{ln(2)}{t_{1/2}}$ (1/sec)**	**Decay Product**
^{129}I	1.57×10^{7}	1.4×10^{-15}	^{129}Xe
^{36}Cl	3.01×10^{5}	7.3×10^{-14}	^{36}Ar
^{226}Ra	1.60×10^{3}	1.7×10^{-11}	^{222}Rn → ^{218}Po → ^{214}Pb → ^{214}Bi → ^{214}Po → ^{210}Pb → ^{210}Bi → ^{210}Po → ^{206}Pb
^{79}Se[a]	$\sim 3.0 \times 10^{5}$	$\sim 7.3 \times 10^{-14}$	^{79}Br
^{99}Tc	2.13×10^{5}	1.0×10^{-13}	^{99}Ru
^{237}Np	2.14×10^{6}	1.0×10^{-14}	^{233}Pa → ^{233}U→ ^{229}Th → ^{225}Ra → ^{225}Ac → ^{221}Fr → ^{217}At → ^{213}Bi → ^{213}Po → ^{209}Pb → ^{209}Bi
^{242}Pu	3.76×10^{5}	5.8×10^{-14}	^{238}U→ ^{234}Th → ^{234}Pa → ^{234}U→ ^{230}Th → ^{226}Ra → ^{222}Rn → ^{218}Po → ^{214}Pb → ^{214}Bi → ^{214}Po → ^{210}Pb → ^{210}Bi → ^{210}Po → ^{206}Pb

a. Note that the National Nuclear Data Center (NNDC - https://www.nndc.bnl.gov/) provides a value of 3.27×10^{5} years from Jorg et al. [2010], but has not fully included the more recent measured values of 2.78×10^{5} years from Dou et al. [2014].

Consider a constant corrosion rate of k and the mass of the layer given by m. Then by a mass balance [Peterson and Dunzik-Gougar, 2011; Van den Akker and Ahn, 2013],

$$\frac{dm}{dt} = -Ak, \tag{II. 1}$$

where all the variables are defined in the Nomenclature section.

For a spherical particle with a layer with inner and outer radii, R_1 and R_2, respectively, in which the inner radius is constant, Eq. (II. 1) becomes

$$\frac{d}{dt}\left(\rho\frac{4}{3}\pi(R_2^3 - R_1^3)\right) = \rho\frac{4}{3}\pi\frac{d}{dt}(R_2^3) = -4\pi k R_2^2 . \qquad \text{(II. 2)}$$

This equation reduces to

$$\rho R_2^2\frac{dR_2}{dt} = -kR_2^2 . \qquad \text{(II. 3)}$$

Eq. (II. 3) can be readily integrated to provide the layer thickness as

$$H(t) \equiv R_2(t) - R_1 = L - \frac{kt}{\rho}, \qquad \left(t \le \frac{\rho L}{k}\right), \qquad \text{(II. 4)}$$

where L is the initial layer thickness at $t = 0$. In Eq. (II.4), the condition in parentheses is required so that corrosion is not considered at or beyond the time that the layer thickness is zero. To get a physical feel for the time to completely corrode the SiC layer, consider

ρ = 3180 kg/m^3,

$k = 4.5 \times 10^{-5}$ and 2.9×10^{-6} g/m^2/day = (5.2×10^{-13} and 3.4×10^{-14} kg/m^2/s), and

$L = 35 \times 10^{-6}$ m.

The corrosion rates k, correspond to the average corrosion rates in brine at 90 °C and 25 °C, respectively from Fachinger et al. [2006]. From Eq. (II. 4),

$$t = \frac{\rho L}{k} = \begin{cases} \dfrac{(3180)(35\times10^{-6})}{5.2\times10^{-13}} = 2.1\times10^{11}\ \text{s} = 6.8\times10^{3}\ \text{years} \\ \dfrac{(3180)(35\times10^{-6})}{3.4\times10^{-14}} = 3.3\times10^{12}\ \text{s} = 1.0\times10^{5}\ \text{years} \end{cases} . \qquad \text{(II. 5)}$$

Thus, the time-scale to corrode the SiC layer varies between ~7,000 and 100,000 years, for temperatures of 90 °C and 25 °C, respectively. These time-scales are given in Table 3. For comparison, a 40 µm thick OPyC layer with a density of 2100 kg/m^3 [Lopez-Honorato, 2008], has a corrosion lifetime of ~1,000,000 years at 90 °C.

Table 3. Time-Scales for processes in 35 μm thick layer of SiC.

Process	Time-Scale Expression	Time-Scale (years)
Diffusion	$\tau_{diff} \equiv \frac{L^2}{\mathcal{D}}$	3,900 ($\mathcal{D} = 10^{-20}$ m^2/s) to 39,000 ($\mathcal{D} = 10^{-21}$ m^2/s)
Corrosion	$\tau_{corr} \equiv \frac{\rho L}{k}$	7,000 to 100,000
Radioactive Decay	$\tau_{dec} \equiv \frac{1}{\lambda} = \frac{t_{1/2}}{ln(2)}$	2,300 to 22,700,000

Because the diffusion time-scale depends on the layer thickness squared, small reductions in the layer thickness by corrosion can have a very significant reduction in the diffusion time-scale, making this process more important. If however the corrosion time-scale is much longer than the diffusion time-scale, then geometry changes need not be directly coupled. In this case the solution given by Gelbard [2003] may be used with the outer radius time-varying.

Of the three process in Table 3, the one with the shortest time-scale will control the release. For the time-scales given in Table 3, the time-scales are generally comparable ranging from thousands to tens of thousands of years. Thus these processes should be modeled simultaneously as is done in this work.

Conversely, if one process has a much longer time-scale than the other two processes, then that one process can be ignored compared to the other two faster processes. For example, ^{129}I has a half-life of 16,000,000 years, which is about two orders of magnitude larger than the corrosion time-scale of 100,000 years, and the diffusion time-scale of 39,000 years for a diffusivity of 10^{-21} m^2/s. Thus radioactive decay of ^{129}I may be ignored for releases by diffusion or corrosion.

This page is intentionally blank

III. Diffusive transport of a decaying radionuclide through a spherical shell barrier that is corroding

Consider a spherical shell silicon carbide barrier with inner and outer radii R_1 and R_2, respectively as shown in Figure 4.

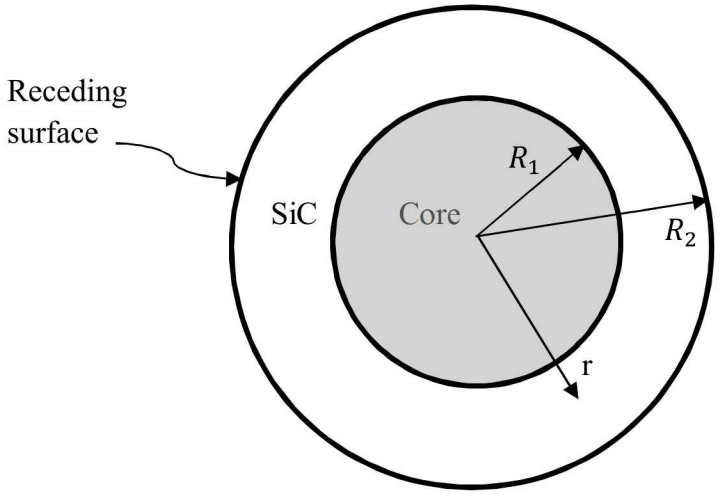

Figure 4. Schematic of spherical shell silicon carbide barrier with inner and outer radii of R_1 and R_2 respectively, and surrounding a core with a spatially uniform fission product concentration. The core is shaded a light gray color. The outer radius decreases with time due to corrosion.

Within the barrier, the concentration of a fission product will vary due to Fickian diffusion and radioactive decay. For spherical symmetry, the concentration is a function of r and t, and is governed by

$$\frac{\partial C}{\partial t} = \frac{\mathcal{D}}{r^2}\frac{\partial}{\partial r}\left(r^2\frac{\partial C}{\partial r}\right) - \lambda C \qquad (R_1 \leq r \leq R_2). \qquad \text{(III. 1)}$$

The core corresponds to the region $0 \leq r \leq R_1$. For TRISO fuel the core consists of the fuel (e.g., UO_2) kernel, the porous pyrolytic carbon layer, and the IPyC layer. The core is not discretized in this simplification as each layer has a diffusivity that is much, much higher than for the SiC layer. In this case, the core concentration is well approximated as spatially uniform, given by $C_1(t)$. The concentration in the barrier at R_1 can be expected to be proportional to the concentration in the core. For convenience in this work, the concentrations at this interface are taken as equal, but the analysis can also be applied if the proportionality constant is known. To maximize the release, the concentration at $r = R_2(t)$ is taken to be zero. For convenience, the initial concentration in the barrier is taken as zero, but the analysis can use an initial concentration profile when available. The boundary conditions are therefore given by

$$C = 0, \text{at } r = R_2(t) \text{ and } t > 0, \tag{III. 2}$$

$$C = C_1(t), \text{at } r = R_1 \text{ and } t > 0, \qquad \text{and} \tag{III. 3}$$

$$C = 0, \text{at } R_1 \leq r \leq R_2 \text{ and } t = 0. \tag{III. 4}$$

The inner radius R_1, is constant. The corrosion rate determines $R_2(t)$, the outer radius as a function of time. It is assumed that R_2 is time-dependent and known, but is independent of the fission product concentration.

A mass balance on the concentration in the core for diffusion into the barrier, and radioactive decay is given by

$$\frac{4}{3}\pi R_1^3 \frac{dC_1}{dt} = 4\pi R_1^2 \mathcal{D} \left(\frac{\partial C}{\partial r}\right)_{r=R_1} - \frac{4}{3}\pi R_1^3 \lambda C_1 \qquad (0 \leq r \leq R_1). \tag{III. 5}$$

The initial condition for the core is given by

$$C_1 = C_1(0) \text{ at } t = 0. \tag{III. 6}$$

Eqs. (III.1) and (III.5) with conditions given by Eqs. (III.2), (III.3), (III.4), and (III.6) comprise the system to be solved. We now introduce two transformations that simplify the coupled system of core and barrier into a single linear partial differential equation and a linear ordinary differential equation.

Let the function $P(r,t)$ be defined such that [Ozisik, 1980]

$$P(r,t) \equiv rC \exp(\lambda t). \tag{III. 7}$$

With this definition, the two terms in Eq. (III.1) with derivatives are given by

$$\frac{\partial C}{\partial t} = \frac{-\lambda P(r,t)\exp(-\lambda t) + \exp(-\lambda t)\frac{\partial P}{\partial t}}{r}, \qquad \text{and} \tag{III. 8}$$

$$\frac{\partial}{\partial r}\left(r^2 \frac{\partial C}{\partial r}\right) = \exp(-\lambda t)\, r \frac{\partial^2 P}{\partial r^2}. \tag{III. 9}$$

Substituting Eqs. (III.7), (III.8), and (III.9) into Eq. (III.1) results in

$$\frac{-\lambda P \exp(-\lambda t) + \exp(-\lambda t)\frac{\partial P}{\partial t}}{r} = \frac{\mathcal{D}}{r^2}\exp(-\lambda t)\, r \frac{\partial^2 P}{\partial r^2} - \lambda \frac{P \exp(-\lambda t)}{r}. \tag{III. 10}$$

This reduces to

$$\frac{\partial P}{\partial t} = \mathcal{D}\frac{\partial^2 P}{\partial r^2}. \tag{III. 11}$$

The boundary and initial conditions become

$$P = 0, \text{at } r = R_2(t) \text{ and } t > 0, \tag{III. 12}$$

$$P = C_1 R_1 \exp(\lambda t), \text{at } r = R_1 \text{ and } t > 0, \text{and} \tag{III. 13}$$

$$P = 0, \text{at } R_1 \leq r \leq R_2(0) \text{ and } t = 0. \tag{III. 14}$$

Eq. (III.11) is the classical one-dimensional Diffusion Equation, but has the advantage that radioactive decay is incorporated implicitly, and is simpler than Eq. (III.1).

The moving boundary can be incorporated into Eq. (III.11) with a transform given by Landau [1950]. This transform preserves the linearity of the Diffusion Equation for a corrosion rate that is independent of the radionuclide concentration. In addition, the spatial domain becomes fixed and normalized from 0 to 1, which is a significant computational advantage. The new time-dependent spatial coordinate is defined by

$$\xi \equiv \frac{R_2(t) - r}{R_2(t) - R_1}. \tag{III. 15}$$

The receding surface is at $r = R_2(t)$, where $\xi = 0$ and $P = 0$. At $r = R_1$, $\xi = 1$ and $P = C_1 R_1 \exp(\lambda t)$.

We now transform Eq. (III.11) from the variables (r, t) to the variables (ξ, T). T is used for time in the new set of variables so that it is clear when the expressions are for the new or old set of variables. Once the derivation is complete, t is substituted for T. Because ξ is a function of both r and t, the transformation is not simple. Therefore, a couple of extra pages for the derivation details are given in this work.

The total differential of P is given by

$$dP = \left(\frac{\partial P}{\partial T}\right)_{\xi} dT + \left(\frac{\partial P}{\partial \xi}\right)_{T} d\xi. \tag{III. 16}$$

The subscript on the brackets is the variable that is being held constant. From Eq. (III.16) the partial derivative of P with respect to t holding r constant is therefore given by

$$\left(\frac{\partial P}{\partial t}\right)_r = \left(\frac{\partial P}{\partial T}\right)_{\xi}\left(\frac{\partial T}{\partial t}\right)_r + \left(\frac{\partial P}{\partial \xi}\right)_{T}\left(\frac{\partial \xi}{\partial t}\right)_r. \tag{III. 17}$$

By taking the partial derivative of ξ with respect to t in Eq. (III.15) we have

$$\left(\frac{\partial \xi}{\partial t}\right)_r = \frac{(R_2(t) - R_1)\frac{dR_2}{dt} - (R_2(t) - r)\frac{dR_2}{dt}}{(R_2(t) - R_1)^2} = \frac{(r - R_1)\frac{dR_2}{dt}}{(R_2(t) - R_1)^2}. \quad \text{(III. 18)}$$

Solving Eq. (III.15) for r results in

$$r = R_2 - \xi(R_2 - R_1). \quad \text{(III. 19)}$$

Substituting Eq. (III.19) for r into Eq. (III.18) results in

$$\left(\frac{\partial \xi}{\partial t}\right)_r = \frac{(R_2 - \xi(R_2 - R_1) - R_1)\frac{dR_2}{dt}}{(R_2 - R_1)^2} = \frac{(1 - \xi)}{(R_2 - R_1)}\frac{dR_2}{dt}. \quad \text{(III. 20)}$$

Substituting Eq. (III. 20) into Eq. (III. 17), and noting that $T = t$, we have that for the left side of Eq. (III.11)

$$\left(\frac{\partial P}{\partial t}\right)_r = \left(\frac{\partial P}{\partial T}\right)_\xi + \frac{(1 - \xi)\frac{dR_2}{dt}}{(R_2 - R_1)}\left(\frac{\partial P}{\partial \xi}\right)_T. \quad \text{(III. 21)}$$

For the right-hand-side of Eq. (III.11),

$$\left(\frac{\partial P}{\partial r}\right)_t = \left(\frac{\partial P}{\partial \xi}\right)_T \left(\frac{\partial \xi}{\partial r}\right)_t + \left(\frac{\partial P}{\partial T}\right)_\xi \left(\frac{\partial T}{\partial r}\right)_t. \quad \text{(III. 22)}$$

However,

$$\left(\frac{\partial T}{\partial r}\right)_t = 0. \quad \text{(III. 23)}$$

Therefore the second partial of P with respect to r is given by

$$\frac{\partial^2 P}{\partial r^2} = \frac{\partial}{\partial r}\left(\frac{\partial P}{\partial r}\right)_t = \frac{\partial}{\partial r}\left(\left(\frac{\partial P}{\partial \xi}\right)_T \left(\frac{\partial \xi}{\partial r}\right)_t\right) = \left(\frac{\partial P}{\partial \xi}\right)_T \left(\frac{\partial^2 \xi}{\partial r^2}\right)_t + \left(\frac{\partial \xi}{\partial r}\right)_t \frac{\partial}{\partial r}\left(\frac{\partial P}{\partial \xi}\right)_T. \quad \text{(III. 24)}$$

This reduces to

$$\frac{\partial^2 P}{\partial r^2} = \left(\frac{\partial P}{\partial \xi}\right)_T \left(\frac{\partial^2 \xi}{\partial r^2}\right)_t + \left(\frac{\partial \xi}{\partial r}\right)_t^2 \left(\frac{\partial^2 P}{\partial \xi^2}\right)_T. \quad \text{(III. 25)}$$

Because the second partial derivative of ξ with respect to r at constant t is zero, Eq. (III. 25) can be reduced further to

$$\frac{\partial^2 P}{\partial r^2} = \left(\frac{1}{R_2(t) - R_1}\right)^2 \left(\frac{\partial^2 P}{\partial \xi^2}\right)_T. \quad \text{(III. 26)}$$

Substituting Eqs. (III.21) and (III.26) into Eq. (III.11) results in a single equation in the (ξ, T) variables with a fixed domain that includes the changing domain effects, and is given by

$$\left(\frac{\partial P}{\partial T}\right)_{\xi} + \frac{(1-\xi)\frac{dR_2}{dt}}{(R_2 - R_1)}\left(\frac{\partial P}{\partial \xi}\right)_{T} = \frac{\mathcal{D}}{[R_2 - R_1]^2}\left(\frac{\partial^2 P}{\partial \xi^2}\right)_{T} \quad (0 \le \xi \le 1, R_2 > R_1). \quad \text{(III. 27)}$$

In general, R_2 and $\frac{dR_2}{dt}$ may be expected to be vary with time as different brine compositions contact the TRISO fuel particle. Nonetheless, if R_2 and $\frac{dR_2}{dt}$ are independent of P, Eq. (III.27) is linear.

The boundary conditions for Eq. (III.27) are for a fixed domain and simplify to

$$P = 0, \text{at } \xi = 0 \text{ and } T > 0, \quad \text{(III. 28)}$$

$$P = C_1(T)R_1 \exp(\lambda T), \text{at } \xi = 1 \text{ and } T > 0, \quad \text{and} \quad \text{(III. 29)}$$

$$P = 0, \text{at } 0 \le \xi \le 1 \text{ and } T = 0. \quad \text{(III. 30)}$$

For convenience, define the recession velocity V by

$$V \equiv -\frac{dR_2}{dT}, \quad \text{(III. 31)}$$

and the initial barrier thickness as

$$L \equiv R_2(0) - R_1. \quad \text{(III. 32)}$$

With these definitions for a positive constant value of $V = k/\rho$,

$$R_2(T) - R_1 = L - VT, \quad \text{(III. 33)}$$

and Eq. (III.27) can be expressed as

$$\left(\frac{\partial P}{\partial t}\right)_{\xi} + \frac{(\xi - 1)V}{(L - Vt)}\left(\frac{\partial P}{\partial \xi}\right)_{t} = \frac{\mathcal{D}}{[L - Vt]^2}\left(\frac{\partial^2 P}{\partial \xi^2}\right)_{t} \quad (L - Vt > 0), \quad \text{(III. 34)}$$

where t has been substituted for T. In this work, V is constant and determined from experimental data. The length scale given by $L - Vt$, is the time-dependent thickness of the barrier. Thus, $(L - Vt)\xi$ corresponds to the radial position distance measured inwards from the outer radius of the barrier. To ensure that there is a barrier thickness to apply Eq. (III.34), the condition $L - Vt > 0$ is imposed.

Eq. (III.34) has the form of a one-dimensional convection-diffusion equation where the effective convective velocity is given by $(\xi - 1)V$, which varies with position. Because $\xi \leq 1$, the effective velocity is negative, except at the core surface. Because increasing ξ corresponds to the inward radial direction, a negative effective velocity corresponds to convection in the outward radial direction. Thus corrosion adds to the flow of fission products radially outwards from the barrier. As time progresses, the barrier thickness given by $L - Vt$ becomes smaller. Because this thickness is in the denominator for both the convective and diffusive term, the effective convective velocity and the effective diffusivity increase with time. The effect is greater for diffusion because the barrier thickness is squared in the denominator of this term on the right side of Eq. (III.34).

At the surface of the core, corresponding to $\xi = 1$, the effective convective velocity is zero. This is consistent with no corrosion effects propagating to the core surface, since the corrosion is occurring at the outer surface of the barrier. Similarly, if the recession velocity V is zero, then the convective term is zero. This is consistent with Eq. (III.34) being reduced to just the diffusion equation, but with ξ as the spatial coordinate instead of r.

To determine the boundary condition on P at $\xi = 1$ from Eq. (III.5), the partial derivative of C with respect to r needs to be expressed in terms of P. From Eq. (III.7),

$$\frac{\partial C}{\partial r} = \exp(-\lambda t)\left[\frac{1}{r}\frac{\partial P}{\partial r} - \frac{P}{r^2}\right]. \qquad \text{(III. 35)}$$

From Eqs. (III.22) and (III.23) we have that

$$\left(\frac{\partial P}{\partial r}\right)_t = \left(\frac{\partial P}{\partial \xi}\right)_T \left(\frac{\partial \xi}{\partial r}\right)_t = \frac{1}{R_1 - R_2}\left(\frac{\partial P}{\partial \xi}\right)_T. \qquad \text{(III. 36)}$$

Substituting Eq. (III.36) into Eq. (III.35) results in

$$\left(\frac{\partial C}{\partial r}\right)_{r=R_1} = e^{-\lambda t}\left[\frac{1}{R_1(Vt - L)}\left(\frac{\partial P}{\partial \xi}\right)_T - \frac{P}{R_1^2}\right]. \qquad \text{(III. 37)}$$

Substituting Eqs. (III.37) and (III.8) into Eq. (III.5) results in the boundary condition at $\xi = 1$ as

$$\left[\frac{dP}{dT}\frac{e^{-\lambda t}}{R_1} - \frac{\lambda e^{-\lambda t}P}{R_1}\right]_{\xi=1} = \frac{3\mathcal{D}e^{-\lambda t}}{R_1}\left[\frac{1}{R_1(Vt - L)}\left(\frac{\partial P}{\partial \xi}\right)_T - \frac{P}{R_1^2}\right]_{\xi=1} - \left(\frac{\lambda e^{-\lambda t}P}{R_1}\right)_{\xi=1}. \qquad \text{(III. 38)}$$

This reduces the boundary condition on P at $\xi = 1$ to

$$\frac{dP}{dt} = \frac{3\mathcal{D}}{R_1}\left[\frac{1}{(Vt - L)}\left(\frac{\partial P}{\partial \xi}\right)_t - \frac{P}{R_1}\right] \qquad (\xi = 1\,), \qquad \text{(III. 39)}$$

with the initial condition

$$P = C_1(0)R_1 \text{ at } t = 0 \text{ and } \xi = 1. \tag{III.40}$$

In Eq. (III.39), $Vt - L$ is negative. The fission product concentration decreases radially away from the inner surface at R_1. However, ξ increases radially inwards towards the inner surface, and thus $\frac{\partial P}{\partial \xi}$ is positive. Thus the term $\frac{1}{(Vt-L)}\left(\frac{\partial P}{\partial \xi}\right)_t$ is negative. Because P and R_1 are positive, the entire right side of Eq. (III.40) is negative or at most zero. This indicates that the fission product concentration in the core will decrease with time.

One useful observation is that the decay constant λ, which is specific to a fission product as given by Table 2, is not used to obtain a solution for P. Thus once P is determined, all the values for C in the barrier and core are determined for any fission product by multiplying by the same factor of $\exp(\lambda t)$ in Eq. (III.7). This feature will be used in Section V to construct a single plot of fission product retention for a range of $\mathcal{D}$ and V that may be used for any fission product given the appropriate value of λ.

In summary, the system to solve is Eqs. (III.34) and (III.39), with boundary conditions given by Eqs. (III.28), (III.29), (III.30), and (III.40). Once P is determined as a function of ξ and t, then Eq. (III.19) may be used to determine P as a function of r and t. Then Eq. (III.7) may be used to determine C as a function of r and t.

This page is intentionally blank

IV. Numerical Discretization

Eq. (III.34) is solved using second-order central finite differences for the spatial derivatives, and the Crank-Nicholson method for time stepping [Press et al., 2007]. For convenience, define

$$A_i^j \equiv \frac{(\xi_i - 1)V}{L - Vt_j}, \tag{IV.1}$$

and

$$B^j \equiv \frac{\mathcal{D}}{\left[L - Vt_j\right]^2}, \tag{IV.2}$$

where the subscript i corresponds to the grid point index, and j corresponds to the time level. Also let h be the spacing in ξ. Then the spatial discretized form of Eq. (III.34) is given by

$$\frac{dP_i}{dt} = B^j \frac{(P_{i+1} - 2P_i + P_{i-1})}{h^2} - A_i^j \frac{(P_{i+1} - P_{i-1})}{2h}. \tag{IV.3}$$

In our notation, the grid point index i, varies from 1 to n, where $i = 1$ corresponds to $\xi = 0$ at which $P = 0$. Grid point n corresponds to the core region, and has the same concentration as the inner surface of the barrier. For the Crank-Nicholson method, let P_i^{j+1} be the value of P at grid point i and time level j+1. Then Eq. (IV.3) becomes for the interior grid points ($1 < i < n$),

$$\frac{2\left(P_i^{j+1} - P_i^j\right)}{\Delta t} = P_{i-1}^j \left[\frac{B^j}{h^2} + \frac{A_i^j}{2h}\right] + P_i^j \left[-2\frac{B^j}{h^2}\right] + P_{i+1}^j \left[\frac{B^j}{h^2} - \frac{A_i^j}{2h}\right]$$

$$+P_{i-1}^{j+1} \left[\frac{B^{j+1}}{h^2} + \frac{A_i^{j+1}}{2h}\right] + P_i^{j+1} \left[-2\frac{B^{j+1}}{h^2}\right] + P_{i+1}^{j+1} \left[\frac{B^{j+1}}{h^2} - \frac{A_i^{j+1}}{2h}\right]. \tag{IV.4}$$

Rearranging Eq. (IV.4) so that the values of P^{j+1} are on the left side, we have that

$$P_{i-1}^{j+1} \left[\frac{\Delta t B^{j+1}}{h^2} + \frac{\Delta t A_i^{j+1}}{2h}\right] - P_i^{j+1} \left[2 + 2\frac{\Delta t B^{j+1}}{h^2}\right] + P_{i+1}^{j+1} \left[\frac{\Delta t B^{j+1}}{h^2} - \frac{\Delta t A_i^{j+1}}{2h}\right] =$$

$$-P_{i-1}^j \left[\frac{\Delta t B^j}{h^2} + \frac{\Delta t A_i^j}{2h}\right] + P_i^j \left[2\frac{\Delta t B^j}{h^2} - 2\right] + P_{i+1}^j \left[\frac{\Delta t A_i^j}{2h} - \frac{\Delta t B^j}{h^2}\right]. \tag{IV.5}$$

For the first grid point at $\xi = h$, we utilize the boundary condition that $P = 0$ at $\xi = 0$. Thus for $i = 1$, $P_{i-1}^{j} = 0$, $P_{i-1}^{j+1} = 0$, and Eq. (IV.5) becomes

$$P_1^{j+1}\left[-2 - 2\frac{\Delta t B^{j+1}}{h^2}\right] + P_2^{j+1}\left[\frac{\Delta t B^{j+1}}{h^2} + \frac{\Delta t A_1^{j+1}}{2h}\right]$$

$$= P_1^{j}\left[2\frac{\Delta t B^{j}}{h^2} - 2\right] + P_2^{j}\left[\frac{\Delta t A_1^{j}}{2h} - \frac{\Delta t B^{j}}{h^2}\right]. \qquad \text{(IV. 6)}$$

Eq. (III.39) for the n-th grid point is given by

$$\frac{dP_n}{dt} = 3\mathcal{D}\left\{\frac{1}{R_1(Vt - L)}\frac{P_n - P_{n-1}}{h} - \frac{P_n}{R_1^2}\right\}. \qquad \text{(IV. 7)}$$

Applying Crank-Nicholson method to Eq. (IV.7) results in

$$P_n^{j+1} - P_n^{j} = \frac{3\mathcal{D}\Delta t}{2R_1}\left[\frac{1}{(Vt^{j+1} - L)}\frac{P_n^{j+1} - P_{n-1}^{j+1}}{h} + \frac{1}{(Vt^{j} - L)}\frac{P_n^{j} - P_{n-1}^{j}}{h} - \frac{P_n^{j+1}}{R_1} - \frac{P_n^{j}}{R_1}\right] \qquad \text{(IV. 8)}$$

The final form of the n–th equation is given by

$$P_{n-1}^{j+1}\left[\frac{3\mathcal{D}\Delta t}{2R_1 h(Vt^{j+1} - L)}\right] + P_n^{j+1}\left[1 - \frac{3\mathcal{D}\Delta t}{2R_1 h(Vt^{j+1} - L)} + \frac{3\mathcal{D}\Delta t}{2R_1^2}\right]$$

$$= P_n^{j}\left[1 + \frac{3\mathcal{D}\Delta t}{2R_1 h(Vt^{j} - L)} - \frac{3\mathcal{D}\Delta t}{2R_1^2}\right] - P_{n-1}^{j}\left[\frac{3\mathcal{D}\Delta t}{2R_1 h(Vt^{j} - L)}\right]. \qquad \text{(IV. 9)}$$

The tridiagonal system of n equations for P_i^{j+1} $(i = 1, 2, \ldots, n)$ is given by Eq. (IV.6) as the first row, Eq. (IV.5) for rows 2 to n-1, and Eq. (IV.9) as the n-th row. This tridiagonal system is solved each time step which does not require iteration [Press et al., 2007].

V. Calculation Results

To demonstrate the coupling of corrosion and diffusion, consider a SiC layer as given in Figure 4 exposed to brine. The conditions are

$$C = 0, \text{at } r = 420\ \mu\text{m and } t \geq 0, \tag{V.1}$$

$$C = C_1(0), \text{at } r = 385\ \mu\text{m and } t = 0, \quad \text{and} \tag{V.2}$$

$$C = 0, \text{at } 385\ \mu\text{m} \leq r \leq 420\ \mu\text{m and } t = 0. \tag{V.3}$$

As given by Eq. (III.34), there must be a finite thickness to the barrier layer which is given by the requirement that $Vt/L < 1$. Therefore the calculations are carried out to Vt/L = 0.9999 with 150 time steps. Once this limit on the simulation is reached, the barrier is assumed to be thin enough so that there is no diffusion barrier. All the results were computed with $n = 50$. Convergence was checked by repeating a calculation with $n = 100$, and there was no noticeable difference. Similarly, there was no noticeable difference when using 100 time steps.

The mass of fission products in the core and barrier at any time is given by

$$M(t) = \frac{4}{3}\pi R_1^3 C_1 + \int_{R_1}^{R_2} 4\pi r^2 C\, dr \tag{V.4}$$

where C is a function of r and t. The effects of radioactive decay are already included in Eq. (V.4) by the determination of C_1 and C. The first and second terms on the right in Eq. (V.4) corresponds to the decaying fission product mass remaining in the core and in the barrier, respectively. If all the fission product mass remains in the core, then with time this mass is given by

$$\frac{4}{3}\pi R_1^3 C_1(0) e^{-\lambda t}\ . \tag{V.5}$$

Thus, the mass fraction of fission products retained in the core plus barrier system is given by

$$F(t) = \frac{\frac{4}{3}\pi R_1^3 C_1(t) + \int_{R_1}^{R_2} 4\pi r^2 C\, dr}{\frac{4}{3}\pi R_1^3 C_1(0) e^{-\lambda t}}. \tag{V.6}$$

The ideal barrier has $F(t)$ approaching unity, which in this limit indicates all the fission product has been retained in the core and barrier system. The retained mass fraction as defined by Eq. (V.6) is given in Figure 5. The integral in the numerator of $F(t)$ is computed using a trapezoidal rule.

As noted at the end of Section III, all the values of C in the numerator of Eq. (V.6) are obtained by multiplying P by $\exp(-\lambda t)/r$. Thus the factor of $\exp(-\lambda t)$ cancels in the numerator and denominator of Eq. (V.6), and the effects of radioactive decay are not included in $F(t)$. Therefore, if $F(t)$ is unity, that does not mean that over time the mass of fission product is the same as the mass initially in the core. The mass of fission product in the core plus barrier system can be determined by using $F(t)$ and is given by

$$\frac{4}{3}\pi R_1^3 C_1(0) e^{-\lambda t} F(t). \qquad \text{(V.7)}$$

Therefore, given a plot of $F(t)$ for a range of $\mathcal{D}$ and τ_{corr}, such as Figure 5, the plot may be used for all the fission products in Table 2 by using the appropriate value of λ in Eq. (V.7). Thus separate plots are not needed for different fission products.

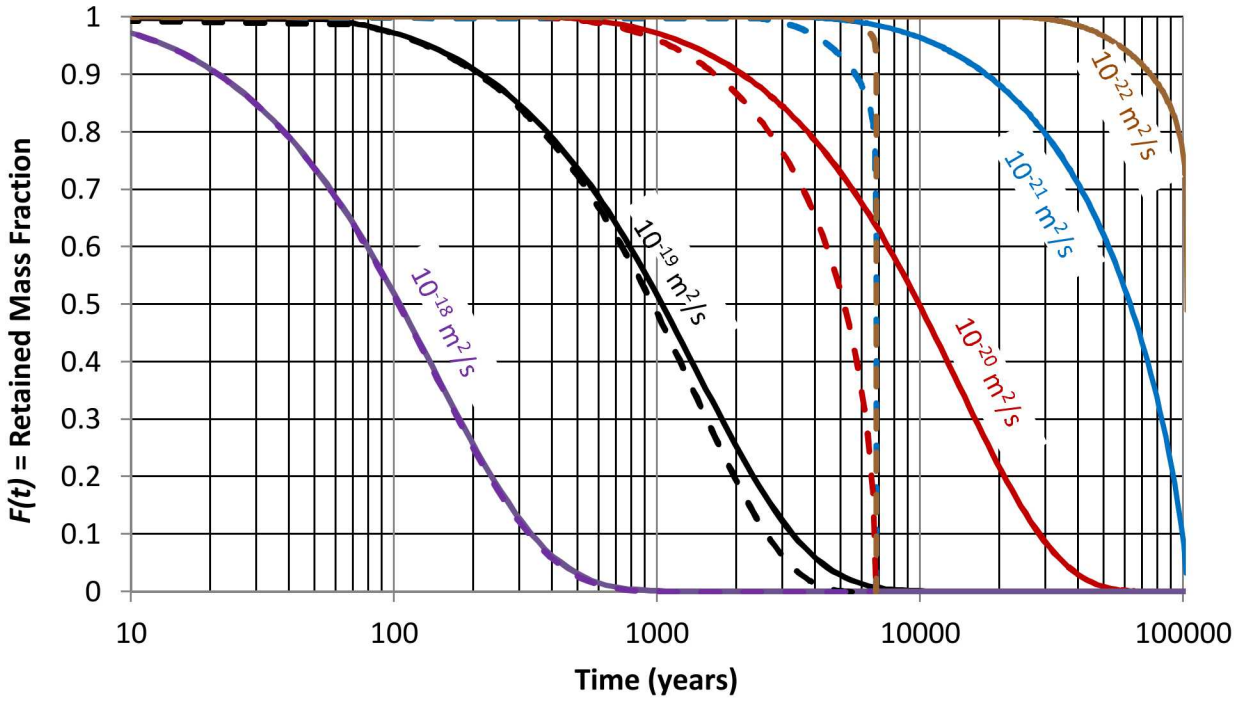

Figure 5. Fraction of fission product mass remaining within the core and corroding SiC barrier as a function of the diffusivity in the barrier and corrosion rate. The diffusivity values are shown in the same color as the lines. Solid lines and dashed lines correspond to corrosion lifetimes of 100,000 years and 7,000 years, respectively.

Based on Figure 3, corrosion rates of $k = 4.5 \times 10^{-5}$ and 2.9×10^{-6} g/m^2/day, correspond to corrosion lifetimes τ_{corr} of about 7,000 and 100,000 years, respectively. Since we have not found bulk diffusivities in SiC at repository temperatures, $F(t)$ is shown in Figure 5 for fission product diffusivities of $\mathcal{D} = 10^{-18}$, 10^{-19}, 10^{-20}, 10^{-21} and 10^{-22} m^2/s. Given these assumed values for $\mathcal{D}$, the basic premise of $\mathcal{D} \ll \mathcal{D}_{core}$ is valid, because the time-scale to diffuse through the pyrolytic carbon layers is orders of magnitude smaller than the time-scale for diffusion through the SiC barrier. Based on Table 3, for diffusivities of 10^{-18} and 10^{-19} m^2/s the diffusion time-scales are 39 and 390 years, respectively. This is much shorter than the shortest corrosion time-scale of 7,000 years for $k = 4.5 \times 10^{-5}$ g/m^2/day. Therefore we expect as shown in Figure 5, that the radionuclide diffuses out of the SiC barrier layer for $\mathcal{D} = 10^{-18}$ and 10^{-19} m^2/s before corrosion removes this layer. Thus there is little difference between the solid and dashed curves of the same color for these diffusivities, indicating that diffusive release is dominant over corrosion removal. The solid and dashed curves correspond to corrosion time-scales of 100,000 and 7,000 years, respectively.

However, for $\mathcal{D} = 10^{-20}$ m^2/s, the diffusion time-scale from Table 3 is 3,900 years. In this case we expect as shown in Figure 5 there are significant differences in the retained fission product mass fraction depending on the corrosion rate. For corrosion time-scale of 100,000 years, which is much longer than the diffusion time-scale, diffusion releases nearly all of the fission product before the SiC layer is removed by corrosion as shown by the red solid curve. However, for corrosion time-scales of 7,000 years, both diffusion and corrosion are important, but complete release occurs essentially when the SiC layer is removed by corrosion as shown by the red dashed curve.

For $\mathcal{D} = 10^{-21}$ m^2/s or smaller, the diffusion time-scale is 39,000 years or longer. Therefore, for a corrosion time-scale of 7,000 years, most of the radionuclide is released by corrosion as shown by the blue dashed curve. Similarly for $\mathcal{D} = 10^{-22}$ m^2/s the diffusion time-scale is 390,000 years, and therefore most of the radionuclide is released via corrosion even for a corrosion time-scale of 100,000 years.

This page is intentionally blank

VI. Conclusions

In this work we analyzed the combined simultaneous effects of bulk (e.g., solid-state) diffusion of a radionuclide through the SiC barrier, barrier corrosion, and radioactive decay for TRISO particles. The analysis is general for a single corroding barrier with specified radionuclide bulk diffusivity and decay rate. From the time-scales for bulk diffusion, corrosion, and decay, estimates were obtained on how each process would affect the radionuclide release. Because we did not find the bulk diffusivities in SiC of the radionuclide of interest at repository temperatures, a broad range of diffusivities was used in the analysis. Release may occur before the SiC barrier has corroded if the bulk diffusivity is more than about 10^{-20} m^2/s. For bulk diffusivity less than 10^{-21} m^2/s there may not be significant diffusional release prior to SiC barrier removal by corrosion.

In the future, the physical characteristics and porous media properties of the TRISO particle layers and of the encapsulating compact graphite matrix (or pebble graphite matrix), are to be constrained for integration into a stochastic model of the entire compact contained TRISO particle fuel degradation. Graphite corrosion as analyzed previously appears to be the slowest process of all and can be ignored to a first approximation relative to aqueous diffusion through the graphite.

Based on the analysis in this work, TRISO fuel is a very robust design for retaining fission products if the protective layers remain intact and preclude radionuclide transport by advection or aqueous-phase diffusion. Measurements have shown that if the layers composed of pyrolytic carbon and silicon carbide are contacted by brine, corrosion of these layers may occur. Even if the corrosion rate measured at 90 °C by Fachinger et al. [2006] is assumed to be applicable over geological time-scales, the outer pyrolytic carbon (OPyC) layer should last more than about 10^6 years. The long lasting OPyC layer would also provide at least some corrosion protection to the silicon carbide (SiC) layer that is covered by the OPyC layer. However, other measurements reported by Fachinger et al. [2006] show that SiC corrodes much faster in brine than does the pyrolytic carbon. Therefore, if the OPyC layer is damaged such that brine contacts the silicon carbide layer ubiquitously, then there is the potential for the corrosion of SiC as analyzed here and concurrent radionuclide release. Whether or not the SiC layer corrodes, there is always a potential release by bulk diffusion through SiC. Protecting the SiC layer from corrosion increases the time needed for diffusion through this barrier. This slow release through the SiC layer provides some safety margin. But quantitative evaluation of the porous media diffusion in the compact graphite matrix and the TRISO layers, at repository conditions is one of the next major steps in this model development.

This page is intentionally blank.

References

Boer, B., Y. M. Kim, W. Wu, A. M. Ougouag, D. McEachern, and F. Venneri, "Inter-comparison of Computer Codes for TRISO-based Fuel Micro-Modeling and Performance Assessment," Proceedings of HTR 2010, Prague, Czech Republic, October 18-20, 2010, paper 159.

Bower, G. R., S. A. Scott, P. A. Demkowicz, "Measurement of kernel swelling and buffer densification in irradiated UCO-TRISO particles," *Journal of Nuclear Materials* **486**, 339-349, 2017.

Cao, F., W. Hao, X. Wang, F. Guo, X. Zhao, N. Rohbeck, and P. Xiao, "Effects of water vapor on the oxidation and the fracture strength of SiC layer in TRISO fuel particles," *Journal of the American Ceramic Society* **100**, 2154-2165, 2017.

Chaou, A. A., A. Abdelouas, G. Karakurt, and B. Grambow, "Aqueous alteration of VHTR fuels particles under simulated geological conditions," *Journal of Nuclear Materials* **448**, 206-216, 2014.

Crank, J., Free and Moving Boundary Problems, Oxford, 1988.

De Bellefon, G. M. and B. D. Wirth, "Kinetic Monte Carlo (KMC) simulation of fission product silver transport through TRISO fuel particle," *Journal of Nuclear Materials* **413** (2) 122-131, 2011.

Demkowicz, P. A., J. M. Harp, P. L. Winston, and S. A. Ploger, "Analysis of Fission Products on the AGR-1 Capsule Components," Idaho National Laboratory, INL/EXT-13-28483, March 2013.

Demkowicz, P. A., J. D. Hunn, S. A. Ploger, R. N. Morris, "Irradiation performance of AGR-1 high temperature reactor fuel," *Nuclear Engineering and Design*, **306**, 2-13, 2016.

Deng, J., H. Ko, P. Demkowicz, D. Morgan, and I. Szlufarska, "Grain boundary diffusion of Ag through polycrystalline SiC in TRISO fuel particles," *Journal of Nuclear Materials* **467**, 332-340, 2015.

Dou, L., S. Jiang, X. Wang, K. Dong, S. Wu, X. Yang, X. Wang, X. Lan, Q. Xia, and M. He, "Measurement of the half-life of ^{79}Se with accelerator mass spectrometry," *Chinese Physics C*, **38** (10), 106204-1 – 106204-4, 2014.

Fachinger, J., M. den Exter, B. Grambow, S. Holgersson, C. Landeman, M. Titov, and T. Podruhzina, "Behavior of spent HTR fuel elements in aquatic phases of repository host rock formation," *Nuclear Engineering and Design* **236**, 543-554, 2006.

Friedland, E., J. B. Malherbe, N. G. van der Berg, T. Hlatshwayo, A. J. Botha, E. Wendler, and W. Wesch, "Study of silver diffusion in silicon carbide," *Journal of Nuclear Materials* **389,** 326-331, 2009.

Friedland, E., N. G. van der Berg, J. B. Malherbe, and W. Wesch, "Investigation of silver and iodine transport through silicon carbide layers prepared for nuclear fuel element cladding," *Journal of Nuclear Materials* **410** (1) 24-31, 2011.

Gelbard, F., "Analytical Modeling of Fission Product Releases by Diffusion from Multicoated Fuel Particles," Sandia National Laboratories, Albuquerque, New Mexico, SAND2002-3966, March 2003. (see Appendix A in this work for an update.)

Hunn, J. D., C. A. Baldwin, T. J. Gerczak, F. C. Montgomery, R. N. Morris, C. M. Silva, P. A. Demkowicz, J. M. Harp, and S. A. Ploger, "Detection and analysis of particles with failed SiC in AGR-1 fuel compacts," *Nuclear Engineering and Design* **306**, 36-46, 2016.

Jorg, G., R. Buhnemann, S. Hollas, N. Kivel, K. Kossert, S. Van Winckel, and C. Gostomski, "Preparation of radiochemically pure ^{79}Se and highly precise determination of its half-life," *Applied Radiation and Isotopes* **68**, 2339-2351, 2010.

Khalil, S., N. Swaminathan, D. Shrader, A. J. Heim, D. D. Morgan, and I. Szlufarska, "Diffusion of Ag along Σ3 grain boundaries in 3C-SiC," *Physical Review B* **84**, 214104, 2011.

Kirchhofer, R., J. D. Hunn, P. A. Demkowicz, J. I. Cole, and B. P. Gorman, "Microstructure of TRISO coating particles from the AGR-1 Experiment: SiC Grain Size and Grain Boundary Character," *Journal of Nuclear Materials* **432**, 127-134, 2013.

Ko, H., J. Deng, I. Szlufarska, and D. Morgan, "Ag diffusion in SiC high-energy grain boundaries: Kinetic Monte Carlo study with first-principle calculations," *Computational Materials Science* **121**, 248-258, August 2016.

Kucera, A., Mathematics of moving boundary problems in diffusion, Ph.D. Thesis, University of Wollongong, Australia, 1985.

Landau, H. G., "Heat Conduction in Melting Solid," *Quarterly Journal of Applied Mathematics* **8**, 81-94, 1950.

Malherbe, J. B., "Diffusion of fission products and radiation damage in SiC," *Journal of Physics D – Applied Physics* **46** (47), 473001, 2013.

Miller, G. K., D. A. Petti, J. T. Maki, "Development of an Integrated Performance Model for TRISO-Coated Gas Reactor Particle Fuel," INEEL/CON-01-01553, Preprint, HTR 2002 Conference, April 22-24, 2002.

Minato, K., T. Oagawa, K. Fukuda, M. Shimizu, Y. Tayama, and I. Takahashi, "Fission Product Behavior in Triso-Coated UO_2 Fuel Particles," *Journal of Nuclear Materials* **208**, 266-281, 1994.

Nabielek, H., H. van der Merwe, J. Fachinger, K. Verfondern, W. von Lensa, B. Grambow, and E. de Visser-Tynaova, "Ceramic coated particles for safe operation in HTRS and in long-term storage," *Ceramic Engineering and Science Proceedings* **30** (10) 193-202, 2010.

Ozisik, M. N., Heat Conduction, Wiley, New York, 1980.

Peterson, J. L. and M. L. Dunzik-Gougar, "Modeling spent TRISO fuel for geological disposal: corrosion and failure under oxidizing conditions in the presence of water," *Progress in Nuclear Energy* **53** (3) 278-284, 2011.

Powers, J. J. and B. D. Wirth, "A Review of TRISO Fuel Performance Models," *Journal of Nuclear Materials* **405**, 74-82, 2010.

Press, W. H., S. A. Teukolsky, W. T. Vetterling, and B. P. Flannery, Numerical Recipes: The Art of Scientific Computing, 3rd edition, Cambridge University Press, 2007.

Rabone, J. E., Lopez-Honorato, and P. V. Uffelen, "Silver and Cesium Diffusion Dynamics at the β-SiC grain boundary Investigated with Density Functional Theory Molecular Dynamics and Metadynamics," *The Journal of Physical Chemistry* **118**, 915-926, 2014.

Rabone, J. and E. Lopez-Honorato, "Density functional theory metadynamics of silver, caesium and palladium diffusion at β-SiC grain boundaries," *Journal of Nuclear Materials* **458**, 56-63, 2015.

Sassani, D., P. Brady, F. Gelbard, L. Price, J. Prouty, R. Rechard, M. Rigali, R. Rogers, A. Sanchez, W. Walkow, and P. Weck, "Inventory and Waste Characterization Status Report and OWL Update," September 24, 2018, M2SF-18SN010309013; SAND-2018-12352 R, Sandia National Laboratories, Albuquerque, NM, 2018.

Shyy, W., H. S. Udaykumar, M. M. Rao, and R. W. Smith, Computational Fluid Dynamics with Moving Boundaries, Dover, 2007.

Sterbentz, J. W., B. Phillips, R. L. Sant, G. S. Chang, and P. D. Bayless, "Reactor Physics Parametric and Depletion Studies in Support of TRISO Particle Fuel Specification for the Next Generation Nuclear Plant, INEEL/EXT-04-02331, Idaho National Engineering and Environmental Laboratory, Idaho Falls, Idaho, September 2004.

Tao, L. N., "A Method for Solving Moving Boundary Problems," *SIAM Journal on Applied Mathematics* **46** (2) 254-264, April 1986.

Van den Akker, B. P. and J. Ahn, "Performance assessment for geological disposal of graphite waste containing TRISO particles," *Nuclear Technology* **181** (3) 408-426, 2013.

APPENDIX A: UPDATE FOR SAND2002-3966

The last paragraph and figure of Section IV of the report SAND2002-3966 (Gelbard, 2003) should be replaced with the following.

The general multilayer solution given by Eq. (IV.9) approaches the two-layer coupled lumped fuel and barrier model given previously in the limit of

$\xi = D_{fuel}(r_3-r_2)^2/[D_{barrier}(r_2-r_1)^2] >> 1$. This is shown as a solid line in Figure IV.2 for the fraction released as given by Eq. (III.21). The curves for ξ equal to 1.0, 0.1, and 0.01 were computed from Eq. (IV.15). The dimensionless time is given by Eq. (III.8) with the diffusivity taken as that for the barrier layer. For ξ greater than about 1.0, the simpler lumped fuel and barrier model is already adequate for determining the release fraction.

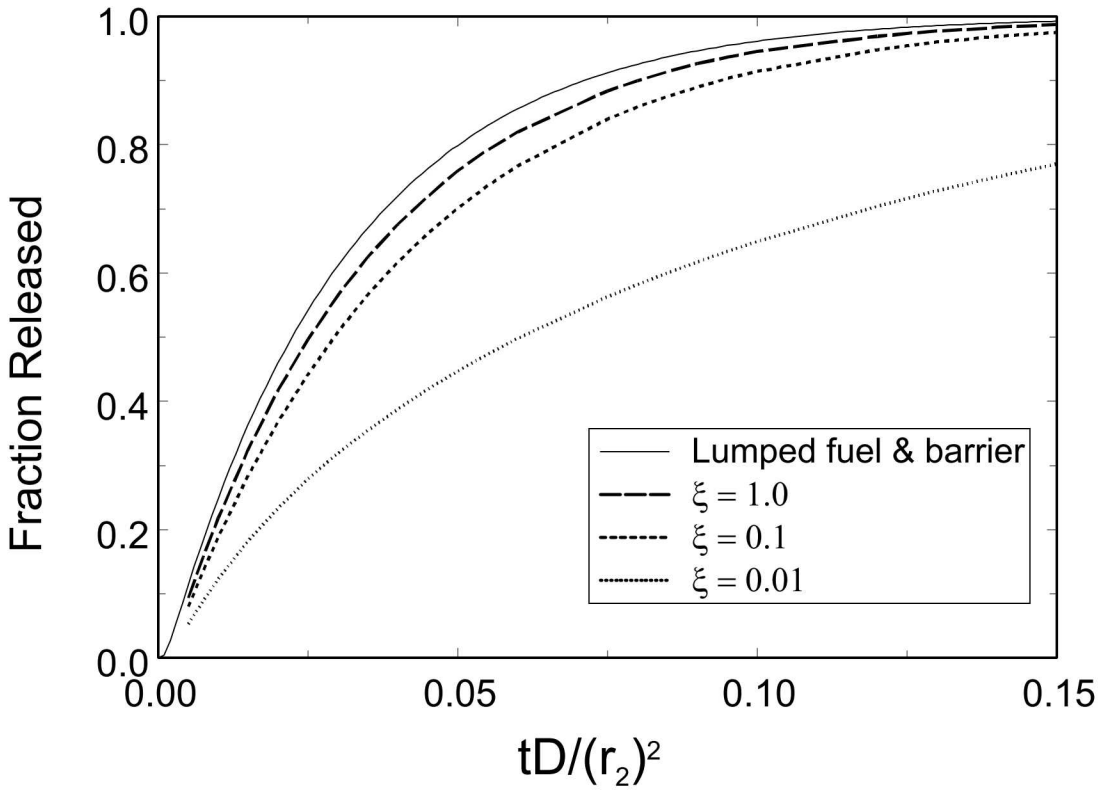

Figure IV.2. Comparison of fraction released for lumped fuel and barrier model, and multilayer model for $r_3/r_2 = 1.10$, and $\gamma_1 = \gamma_2 = 1$. The limit of $\xi >> 1$ is the solution given in Eq. (III.21) as the lumped fuel and barrier model.

This page is intentionally blank

DISTRIBUTION

Internal Sandia National Laboratories Electronic Distribution

Mail Stop	Name	Organization
0736	Peter Swift	8840
0747	Geoffrey Freeze	8843
0747	Robert MacKinnon	8844
0747	Philippe Weck	8845
0779	Kevin McMahon	8842
0779	Sylvia Saltzstein	8845
0779	Edward Mateo	8842
0899	Technical Library	9536 (electronic copy to sanddocs@sandia.gov)

External Electronic Distribution

Jorge Monroe-Rammsy	U. S. Department of Energy NE-81, 232 Energy Way North Las Vegas, NV 89030 (Jorge.Monroe-Rammsy@nuclear.energy.gov).
Mark Tynan	U. S. Department of Energy NE-81, 232 Energy Way North Las Vegas, NV 89030 (mark.tynan@nuclear.energy.gov).
William Spezialetti	U. S. Department of Energy NE-81, 232 Energy Way North Las Vegas, NV 89030 (bill.spezialetti@nuclear.energy.gov).
Timothy Gunter	U. S. Department of Energy NE-81, 232 Energy Way North Las Vegas, NV 89030 (timothy.Gunter@nuclear.energy.gov).
William Boyle	U. S. Department of Energy NE-8, 19901 Germantown Road, Germantown, MD 20874 (william.boyle@nv.doe.gov).


Sandia National Laboratories